Predictions in Ungauged Basins: Promise and Progress (Proceedings of symposium S7 held during the Seventh IAHS Scientific Assembly at Foz do Iguaçu, Brazil, April 2005). IAHS Publ. 303, 2006.

Frequency-domain analyses of GPR waveforms: enhancing near-surface observational capabilities

GUY SERBIN[1] **& DANI OR**[2]

1 *Department of Plants, Soils, and Biometeorology, Utah State University, Logan, Utah 84322-4820, USA.*
now at: Geosciences Dept, University of Rhode Island, Kingston, Rhodes Island 02881 USA
guy.serbin@gmail.com

2 *Department of Civil and Environmental Engineering, University of Connecticut, 261 Glenbrook Road, Unit 2037, Storrs, Connecticut 06269-2037, USA.*
now at: Laboratory of Soil and Environmental Physics (LASEP), School of Architectural, Civil and Environmental Engineering (ENAC/ISTE), Ecole Polytechnique Federale de Lausanne (EPFL), Bâtiment GR 2 (room 554), CH-1015 Lausanne, Switzerland

Abstract Greenhouse and field wheat canopy time domain (TD) ground-penetrating radar (GPR) measurements were analysed in the frequency domain (FD) using Fast Fourier Transforms (FFT). FFTs of top canopy, soil surface, and subsurface Al-foil termination reflections and entire profiles were compared with TD surface reflection magnitudes (SR) and signal propagation time (PT) estimated water contents Θ_v. Direct relationships were found between TD and FD SR magnitudes and Θ_v, and indirect relationships between TD SR and PT values and FD SR components. GPR profiles FFTs showed interference patterns attributed to interactions between reflecting layers within the profile. FD profile radar backscatter coefficient σ^0 values at 430 MHz (P-band) and 1.26 GHz (L-band) showed that near-surface reflective objects biased results, particularly at lower frequencies where signal penetration depths were greater. The final results show that a single monostatic horn antenna with sufficient bandwidth can determine near-truth radar backscattering parameters for air- and spaceborne platforms.

Key words canopy scattering; horn antenna; radar remote sensing; soil water content

INTRODUCTION

Narrowband frequency domain (FD) synthetic aperture radar (SAR) and scatterometer systems are frequently used for acquisition of data from vegetation canopies, soil surfaces, and subsurfaces (Berlin *et al*., 1986; Ulaby *et al*., 1996; Blumberg *et al*., 2000, 2002; Paloscia, 2002; Daniels *et al*., 2003), as they allow for rapid scanning or imaging of large areas at relatively low monetary costs. However, one main disadvantage of these systems is that they collapse all vegetation canopy, soil surface, and subsurface backscatter contributions into single values, requiring models to explain parameter contributions to the backscattered signal.

Recent research utilized ultrawideband (UWB) time domain (TD) ground-penetrating radar (GPR) with suspended monostatic antennas for measurement of near-surface soil water content and vegetation canopy dynamics (Lambot *et al*., 2004a,b; Serbin & Or, 2003, 2004, 2005), and Serbin & Or (2003, 2004, 2005) showed that GPR with a 1 GHz horn antenna allowed for continuous measurement of soil water content and vegetation canopy dynamics within a well defined footprint.

Bare soil TD GPR measurements by Serbin & Or (2003) showed differing drainage behaviours for differing soil textures, and illustrated the effects of temperature and texture upon bulk soil permittivity ε_b. Greenhouse GPR measurements of a dwarf wheat canopy (Serbin & Or, 2003, 2004, 2005) showed that soil water content Θ_v inferences from GPR measured surface reflectivity (SR) were affected by leaf area index (*LAI*) above a minimal value, LAI_0. Once $LAI > LAI_0$, maximal (post-irrigation) SR-Θ_v values decreased with increasing *LAI* according to Beer-Lambert relationships, while Θ_v inferences from GPR signal propagation times in the soil (PT) were unaffected. Canopy removal resulted in SR values exceeding or being in agreement with PT values. Canopy reflections became visible during the growing season and corresponded to phenological measurements. Field measurements reported in Serbin & Or (2004) showed no canopy effects on SR as the wheat *LAI* never exceeded LAI_0.

All TD signals and reflections may be decomposed to their FD components via use of the Fast Fourier Transform (FFT) technique, allowing for analyses of specific reflections and waveform profiles in the FD. This allows for comparison between narrowband FD radar and wideband GPR systems assuming that they utilize the same frequencies.

This study aims to: (a) study the relationship between TD canopy, surface, and subsurface reflections, and entire profiles and their FD components; and (b) use FD GPR information to assess potential backscatter as would be seen from a down-(nadir-) looking scatterometer system.

THEORETICAL CONSIDERATIONS

TD acquisition of soil dielectric properties via GPR

Commercially available GPR units provide TD measurements that are analogous to those of the widely used time domain reflectometry (TDR) technique (Topp *et al*., 1980; Serbin & Or, 2003). GPR TD waveforms depicted in Fig. 1(a) consist of three distinct regions—antenna, air, and soil. Antenna reflections are caused by impedance mismatches within the antenna and the air. Voltage changes in the air are caused by the near field of the antenna (Balanis, 1982) and reflecting vegetation canopy elements. Major reflections will occur at the soil surface and wherever strong subsurface dielectric discontinuities exist.

The last antenna reflection voltage, V_{ant}, surface reflection voltage, V_{surf}, the antenna-surface propagation time t_{air}, and surface-subsurface propagation time t_p are shown in Fig. 1(a). Canopy reflections (CR) from two canopy layers are boxed in. CR amplitudes are considerably smaller than other reflections of interest.

Dielectric properties via surface reflectivity (SR)

TD SR measurements utilize the antenna voltage and free-space corrected TD SR voltage, V_{surf}, relative to that of a flat metal surface (flat plate), V_{fmp}, to determine the reflection coefficient, $\Gamma(t)$:

$$\Gamma(t) = -\frac{V_{surf}}{V_{fmp}} \tag{1}$$

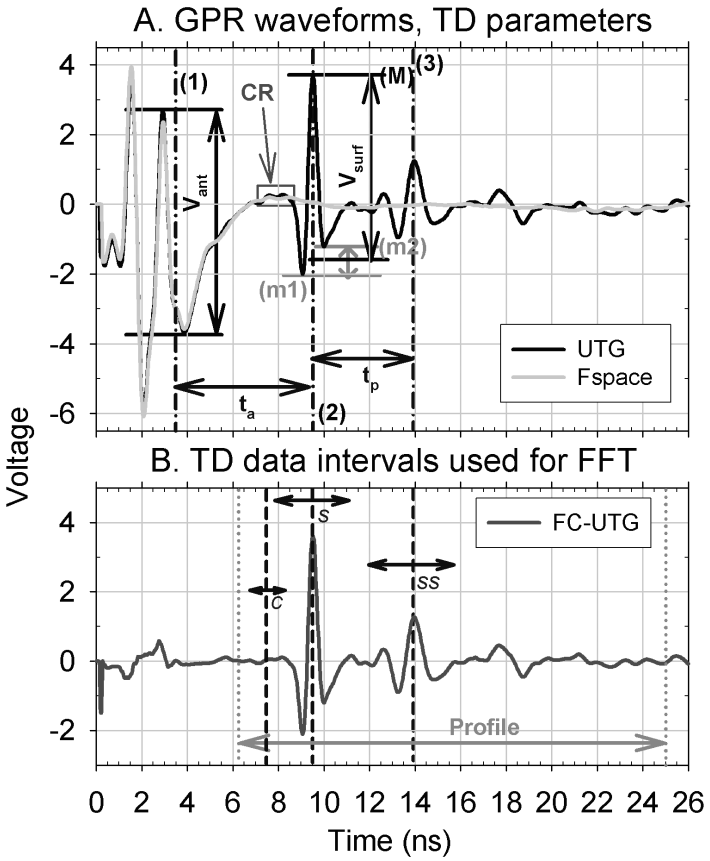

Fig. 1 (a) GPR waveforms from the greenhouse wheat plot (UTG) and a free space calibration (Fspace). (1), (2), and (3) denote antenna-air, air-soil, and soil-Al foil interfaces, respectively. t_a and t_p denote travel time through air and soil, respectively. Important reflection voltages are those of the antenna, V_{ant}, and the soil surface, V_{surf}. V_{surf} is calculated from the Ricker wavelet maximum (M) and minima (m1, m2). CR denotes canopy reflections. (b) Free space corrected waveform (FC-UTG) and reflections/ intervals used for FFT analysis. Vertical dashed lines with intersecting double-ended arrows denote canopy (*c*), surface (*s*), and subsurface (*ss*) reflections analysed; the interval between the vertical dotted lines at 6.25 ns and 25 ns denotes range used for profile FFTs.

where the corrected voltages are determined via:

$$V_c(t) = V(t)\frac{V_{ant,fmp}}{V_{ant,meas}} - V_{air}(t)\frac{V_{ant,fmp}}{V_{ant,air}} \text{ (Volt)} \qquad (2)$$

where the *c*, *air*, and *meas* subscripts denote corrected, free-space, and measurement values, respectively. For clarification purposes, SR measurements should be assumed to be TD in nature unless explicitly stated otherwise. Antenna voltages are used to correct for temperature-induced changes in antenna impedance, and subtraction of scaled free-space waveforms correct for system clutter and near-field effects (Fig. 1(b)), allowing for more accurate determination of V_{surf} and FFT analyses (Balanis, 1982; Serbin & Or, 2005). Flat plate measurements were acquired at the end of experiments by covering the soil surface with thick aluminum foil and then acquiring GPR waveforms. $\Gamma(t)$ may be used to determine ε_b at normal incidence via (Ulaby, 1999):

$$\varepsilon_b = \varepsilon_n \left(-\frac{\Gamma(t)-1}{\Gamma(t)+1} \right)^2 \tag{3}$$

and Θ_v as a function of ε_b may then be determined via the Topp *et al*. (1980) or other relationships, depending on soil composition and frequency considerations.

Dielectric properties via propagation time (PT)

Radar PT measurement of soil water content is possible when a well-defined subsurface reflection exists at a known depth L, such as an interface between two different soil types or between a soil and a metal surface, allowing for t_p to be used to calculate ε_b (Topp *et al*., 1980):

$$\varepsilon_b = \left(\frac{ct_p}{2L} \right)^2 \tag{4}$$

where c is the speed of light in a vacuum (~3×10^8 m s^{-1}). It should be noted that PT measurements are strictly TD.

Radar backscatter from soil and canopy

Polarimetric SARs and scatterometers measure the radar cross-section (RCS), σ^0, which is determined from a power or voltage ratio. σ^0 collapses the responses of all scattering elements into one value, σ^0_{tot} (Dobson & Ulaby, 1986b):

$$\sigma^0_{tot} = \sigma^0_{surf} + \sigma^0_{vol} + \sigma^0_{\text{int}} \tag{5}$$

where the *surf*, *vol*, and *int* subscripts denote the contributions of the soil surface, vegetation canopy volume scattering, and soil surface-vegetation canopy interaction, respectively, to total RCS. The soil surface contribution is a function of the bare soil surface power ratio RCS σ^0_{soil} attenuated via a Beer-Lambert canopy with an optical depth τ:

$$\sigma^0_{surf} = \sigma^0_{soil} \exp(-2\tau \sec\theta) \tag{6}$$

where σ^0_{soil} may be determined via a number of theoretical and semi-empirical models, and includes contributions from the surface and subsurface (Dobson & Ulaby, 1986b; Fung, 1994; Oh *et al*., 1994; Dubois *et al*., 1995; Ulaby *et al*., 1996). Since the soil may be comprised of multiple scattering layers, the σ^0_{soil} term may be expanded to:

$$\sigma^0_{soil} = \sigma^0_{soil,0} + \sigma^0_{soil,1} + \cdots + \sigma^0_{soil,n} \tag{7}$$

where the index numbers in the subscript of σ^0_{soil} denote dielectric interfaces, such that 0 is the air–soil surface boundary, 1 is the first subsurface dielectric interface, and on

to subsurface interface *n*. The canopy volume component results from backscattered radiation occurring from vegetation canopy elements (leaves, stalks, fruit, etc.), and the interaction component denotes multiple scattering between the soil surface and canopy components (Dobson & Ulaby, 1986a,b).

MATERIALS AND METHODS

GPR setup

Remote measurements of the soil surface utilized a Penetradar Corp. IRIS-L GPR unit and a 1 GHz centre frequency 30 AGC monostatic horn antenna (Niagara Falls, New York, USA) with a pulse width of 1 ns and frequency components from 50 MHz to 2.5 GHz, as determined using a FFT of the input monocycle signal. The horn antenna illuminated an elliptical pattern on the soil surface with an area that increased with height. The acquired GPR waveforms were 1600 data points (40 ns) in length. The system was monitored to eliminate waveform drifting.

Greenhouse study

The radar unit was deployed in a greenhouse to measure soil water drying patterns during a growing season of wheat canopy. We planted a dwarf wheat cultivar (USU 9-2-2) with maximal canopy height h_c of 0.4 m to facilitate antenna placement at 1 m above the soil surface on a secured stationary mast, as to measure through a "uniform" canopy. Wheat was planted in a 1.44 m^2 square planter. The planter was filled with an artificial peat-perlite mixture of a very low bulk density (0.14 kg m^3) to a depth of 0.14 m, above a 1 cm thick layer of gravel. The bottom of the planter was terminated with aluminium foil to reflect radiation and mark the location of the bottom for PT measurements. A photograph of the setup may be seen in Fig. 2(a). GPR measurements were acquired every 30 min starting 6 days after planting. After 25 days water was applied via flood irrigation. h_c was monitored every few days using a tape measure. At 58 days after planting the canopy was removed and biophysical parameters measured, including *LAI*. *LAI* and h_c were assumed to be directly related to one another. The bare soil was flood irrigated the same day and measurements acquired for 13 days afterward. Θ_v was validated gravimetrically. The ε_b–Θ_v relationships used in this study were determined by Serbin & Or (2005) to be:

$$\Theta_v = 0.2386 \ln(\varepsilon_b) - 0.1689 \quad (m^3\ m^{-3}) \tag{8}$$

Field study

Field measurements utilized the Yecora Rojo wheat cultivar with a maximal h_c of 0.6 m. The soil used in this study was Millville silt loam, and was separated into two sections, namely a terminated and an unterminated section. The terminated section had a subsurface layer of punctured thick Al foil at a depth of 0.31 m, which was not

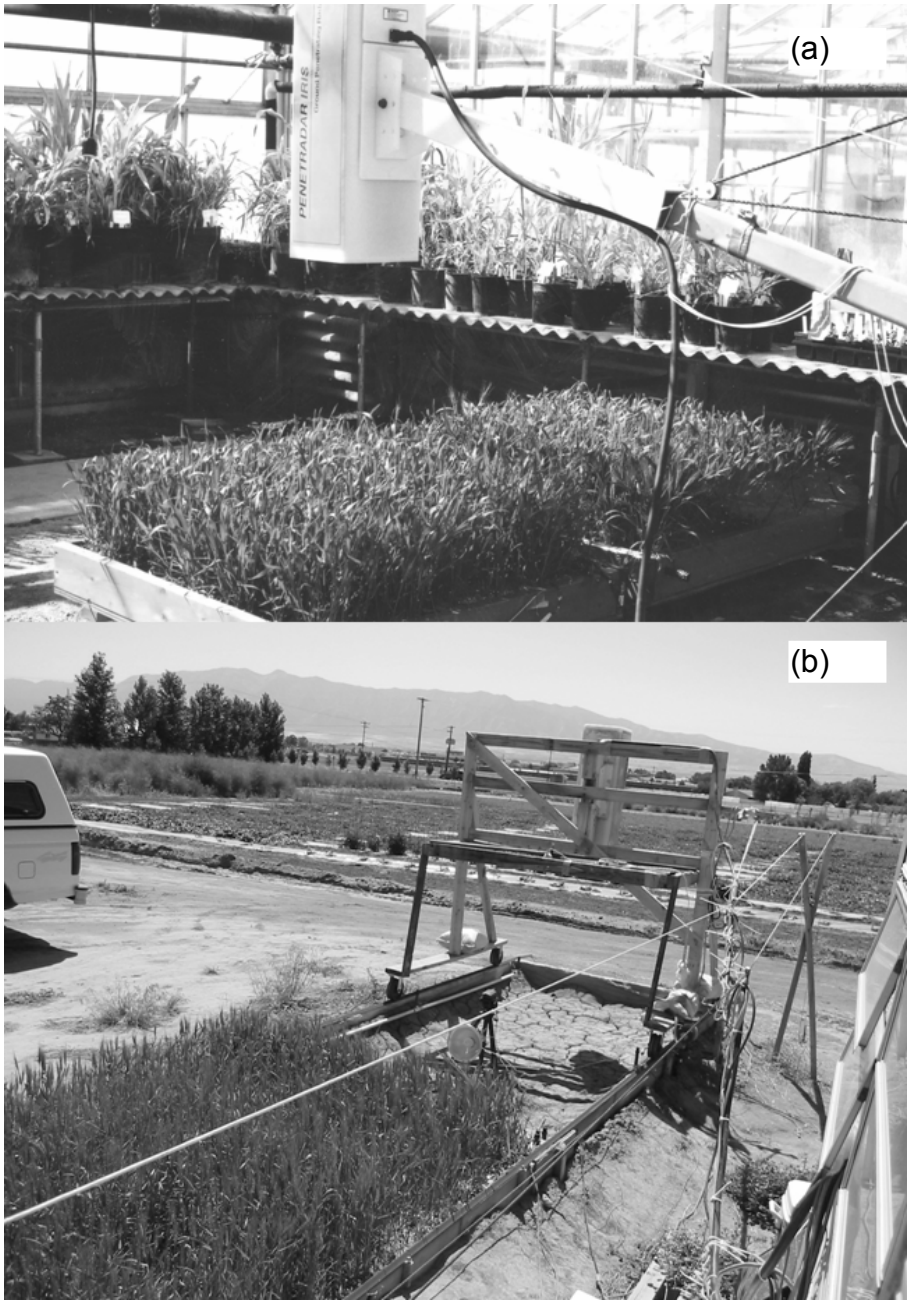

Fig. 2 Photographs of measurement setups in (a) the greenhouse and (b) the field. Figure reproduced from Serbin & Or (2004), with permission.

present in the unterminated layer. Concurrent measurements were acquired every 10 min via a motorized cart, with the antenna suspended at a height of 1.25 m above the soil surface, as seen in Fig 2(b). Θ_v and h_c were measured via TDR and tape measure, respectively. After 61 days of growing the canopy was cut and bare soil measurements began. Biophysical measurements were also acquired. The Topp *et al*. (1980) ε_b–Θ_v relationships were used in this study for estimation of soil water content:

$$\Theta_v = -0.053 + 0.0292\varepsilon_b - 5.5\cdot10^{-4}\varepsilon_b^2 + 4.3\cdot10^{-6}\varepsilon_b^3 \ (\mathrm{m^3\,m^{-3}}) \quad (9)$$

Advanced processing of GPR data

Following time domain analyses of GPR data such as SR- and PT- determination of ε_b and Θ_v, TD GPR waveform data were converted to FD data via FFT of 4096 zero-padded data point sets, outputting complex FD data at increments of 9 765 625 Hz. FFT analyses were performed on the top canopy, surface, and subsurface reflections for greenhouse data (Fig 1(b)). FFTs of air and soil profiles for the greenhouse and field wheat data were also performed from 6.25 ns to 25 ns. Flat plate calibrations were also converted to FD, with the first 300 FD data points being saved. Whole profile responses were determined at 430 MHz and 1.26 GHz, as these correspond with frequently used P- and L-band SAR and scatterometer systems, respectively. Voltage magnitudes V_{abs} in millivolts were determined via:

$$V_{abs}(f) = |V(f)| \quad \text{(Volt)} \tag{10}$$

and radar cross sections σ^0 were calculated via:

$$\sigma^0(f) = 20\log\left(\left|\frac{V_{meas}(f)}{V_{fmp}(f)}\right|\right) \quad \text{(dB)} \tag{11}$$

where $V_{fmp}(f)$ is the frequency domain voltage reflected from the flat metal plate calibration.

RESULTS AND DISCUSSION

Greenhouse measurements

Figure 3 shows the relationships between measured TD results and the FD components of specific reflecting/scattering elements in the canopy and soil profile that affect these measurements. TD SR- and PT-Θ_v inferences (which are discussed in more detail in Serbin & Or (2004, 2005)) may be seen in Fig. 3(a). These data show that as time increases from planting to cutting (as denoted by the vertical line in Fig. 3), maximal SR values decrease with increase in *LAI*, whereas, PT remains unaffected. With this increase in *LAI* an increase in the intensity of canopy reflections also came, as seen in Fig. 3(b). Initially, these reflections, which were very weak and not always discernable, were "piggybacked" on the leading edge of the surface reflection wavelet. Canopy reflections typically centred around 1.2~1.3 GHz throughout the measurements, albeit that between days 47–53 there was a shift toward lower frequencies, as during this time the top canopy reflection was becoming detached from (and thus, overlapping with) the leading edge of the surface reflection (Serbin & Or, 2004, 2005). It should be noted that h_c is a measure of the tallest plants in the canopy; the average plant height in this study was about 0.3 m.

Surface reflection components (Fig. 3(c)) show centre frequencies of about 800 MHz and intensities that are inversely and directly related to *LAI* and SR-Θ_v, respectively. As expected, the canopy effects seen on TD SR data may also be seen on FD data as well, with decreased reflection magnitudes with increasing *LAI*. Following canopy removal a large increase in FD SR magnitude may be seen due to the absence of an overlying canopy to scatter the radiation.

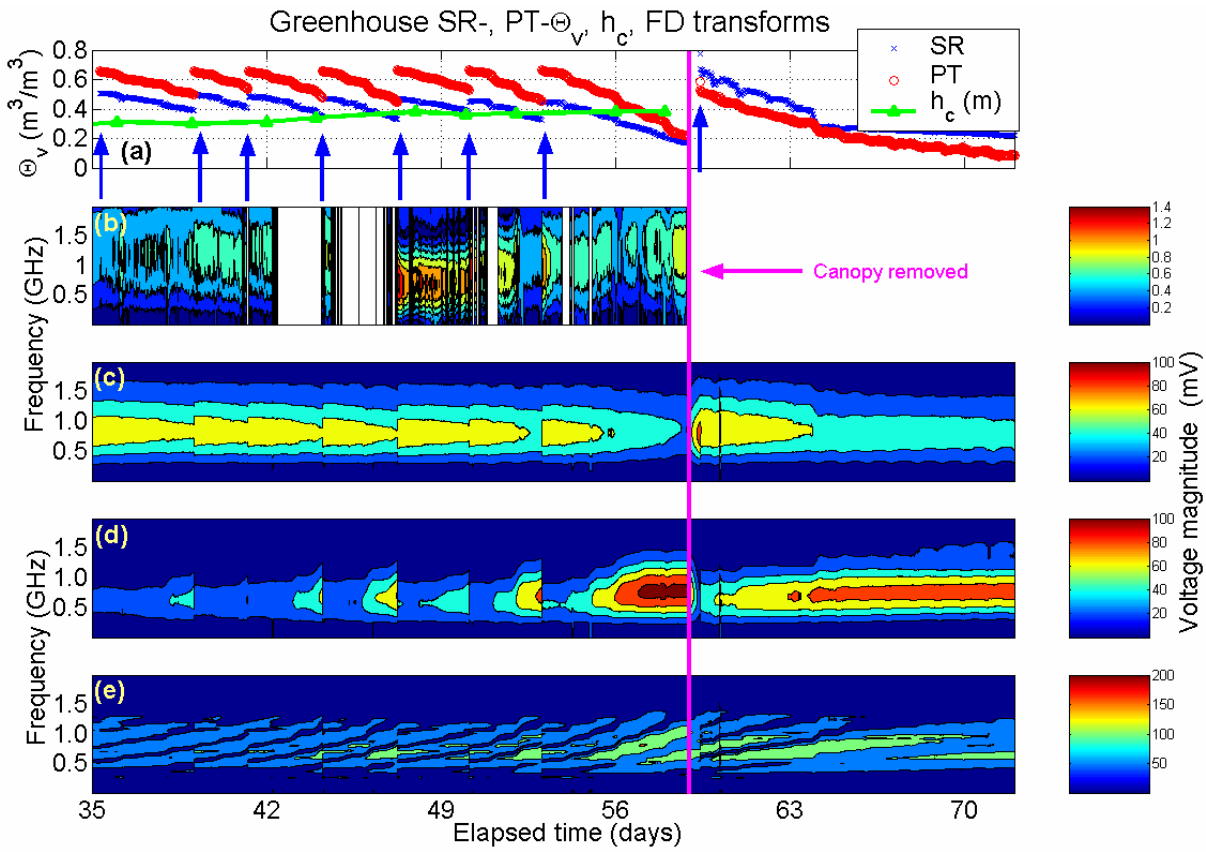

Fig. 3 (a) Time domain SR- and PT- derived Θ_v, and measured h_c. Flood irrigation events are denoted by vertically pointing arrows, canopy removal by vertical line on day 58. FD voltage magnitudes for (b), top canopy layer; (c), soil surface; (d), subsurface Al termination reflections; and (e) entire profile from 6.25 ns to 25 ns. Please note that the colour bars for each contour map are scaled differently.

In the advanced stages of drying the very low-density bare peat-perlite mixture dried out, and the top soil layer became desiccated, such that it had a ε_b similar to that of air, resulting in SR estimates occurring from beneath the soil surface. This is evidenced by both an apparent increase in t_a and little noticeable change in SR as seen for days 65–72, effectively causing a decrease in the effective electrical length of the soil profile, as evidenced by decreasing PT measurements and in Fig. 3(a) and by the downwards shift in intensity as seen in Fig. 3(c).

Subsurface reflectivity (Fig. 3(d)) also seemed to be affected by both the presence of the canopy and by Θ_v, albeit for different reasons. As expected, the intensity of the subsurface Al-termination reflection was inversely related to Θ_v, hence the drier the soil became the brighter this layer appeared to the radar. Interestingly enough, this termination was brighter to the radar in the advanced stages of drying, with the existence of the canopy than without, unlike the surface reflection, suggesting that while canopy elements such as seed heads and leaves may have served to scatter the higher frequencies which comprised the surface reflection, vertically oriented vegetation elements such as stalks served to help confine or collimate the radar footprint at lower frequencies, minimizing air spreading losses, and thus, improving signal strength (Ulaby, 1999; Du *et al*., 2000).

FFTs of the TD waveform profiles from 6.25 ns to 25 ns (Fig. 3(e)) show "rippling" patterns which correspond to constructive and destructive interference patterns between the returning waves from the canopy, surface, and subsurface. Each ripple appears to last 5–7 days. Furthermore, the addition of specific FFTs of canopy, surface, and subsurface resulted in identical results to that of the profile FFT, showing that the σ^0 relations in (7) are valid and indeed additive. Canopy removal also appeared to have an effect on the profile FD values, particularly with respect to the duration of a ripple, as the two ripples which developed after the cutting of the canopy and subsequent irrigation appeared to last over 10–12 days in their drift across the frequency spectrum.

Figure 4 expands on TD and FD radar responses by looking at SR and PT responses for days 52.5–66.5 after planting (Fig. 4(a)) and corresponding FD profile responses at 430 MHz (P-band) and 1.26 GHz (L-band) (Fig. 4(b)). Comparison between these two data sets shows little apparent correlation between measured TD SR or PT and profile FD response, most probably due to the existence of the subsurface terminating layer. However, there does exist evidence of strong destructive interference at L-band on days 56 and 58 in which serious drops in σ^0 of over 20 dB occurred. A further 8 dB drop in L-band σ^0 was also seen on day 63 immediately prior to a measured decrease in both SR and PT.

Field wheat measurements

TD field measurements of wheat canopy and bare soil over terminated (TM) and unterminated (UTM) subsurfaces and FD profile transforms of these data may be seen

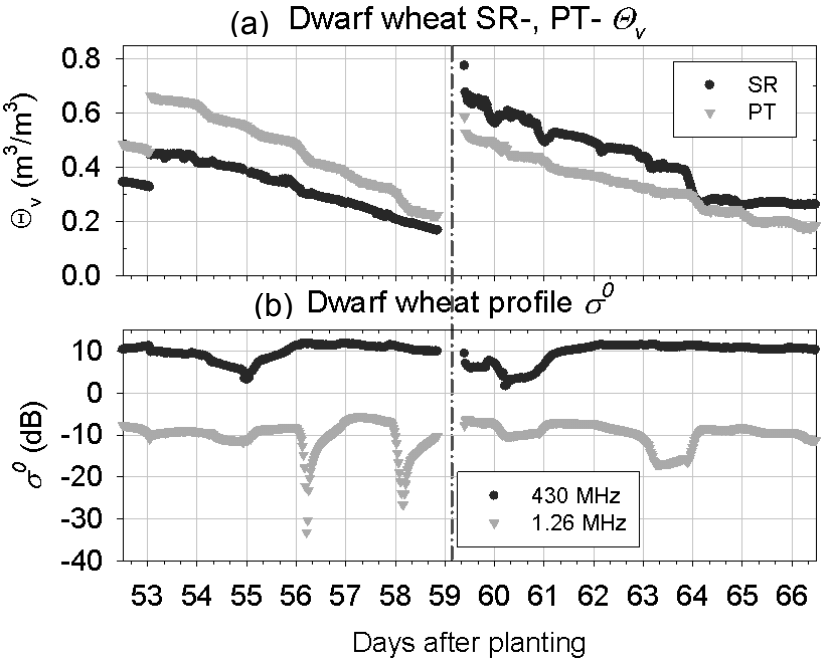

Fig. 4 (a) SR, PT greenhouse drying curves, (b) σ^0 of entire profile at 430 MHz and 1.26 GHz. Dash-dot line denotes time of canopy removal.

in Fig. 5. TD SR data, along with data from a horizontally placed TDR probe at 2 cm depth may be seen in Fig. 5(a). No useful PT data from TM were acquired due to the lack of a clear subsurface reflection, which was due to the electrical conductivity of the soil and presumably also air spreading losses (Ulaby, 1999). The TM and UTM sections showed similar drying patterns, albeit that TM appeared to be wetter for several days following the flood irrigation event. Both TD SR and TDR Θ_v estimates showed clear effects from a flood irrigation event on day 53. However, a rainstorm that occurred on days 63–64 registered only with TD SR Θ_v measurements, suggesting that this rainfall event only penetrated the top cm or less of the soil profile. Removal of the canopy (which is denoted in the figure by a dash-dot line) appeared to have little or no effects on SR as the $LAI < LAI_0$ for the wheat stands. Likewise, this is echoed in FD σ^0 responses for TM (Fig. 5(b)) and UTM (Fig. 5(c)), where canopy removal showed no clear effect for either band. The TM P- and L-band σ^0 responses (Fig. 5(b)) showed similar behaviours for initial drying as seen up to day 60, after which was a divergence, with L-band continuing to decrease and P-band increased. The rainfall event just before midnight on days 63–64 caused an increase and decrease in measured L- and P-band σ^0 values, respectively.

UTM P- and L-band σ^0 responses (Fig. 5(c)) tend to follow those of the TD SR response, albeit that the L-band response is much greater in range and closer in pattern to the SR than P-band. Furthermore, there are clear temporal differences as to the

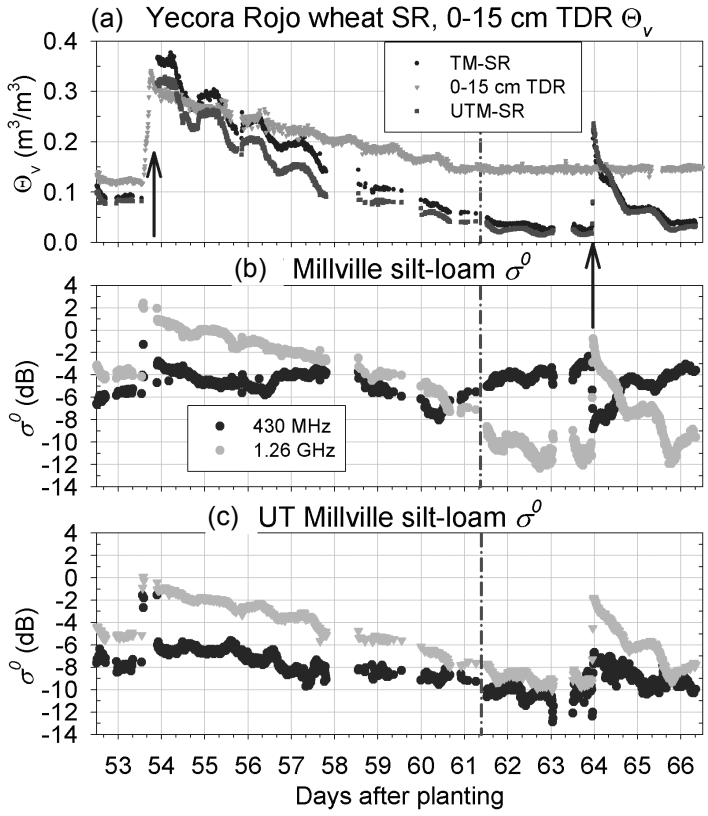

Fig. 5 (a) SR- and TDR- Θ_v estimates. (b) Measured P- and L- band σ^0 for the TM and (c) UTM plots. Dash-dot line denotes time of canopy removal; upward pointing arrows denote irrigation or rainfall events.

occurrence of diurnal σ^0 minima and maxima, suggesting either differing depth sensitivity, sensitivity to bound water partitioning (Serbin & Or, 2003), or both.

The differences seen in the P-band between the TM and UTM σ^0 values were clearly due to the existence or non-existence of a strong subsurface reflector, in this case, Al foil. While it is clear that the L-band signals did not penetrate to the depth of the Al termination, the P-band signals did once the Θ_v of the soils sufficiently decreased, lowering ε_b and electrical conductivity (and thus, electrical length and energy losses), resulting in this subsurface layer becoming increasingly bright on the TM side. Furthermore, this suggests that FD analysis could be used to further the detection capabilities of existing radar systems, particularly in cases where subsurface reflections may not be much different from existing system clutter.

SUMMARY AND CONCLUSIONS

The UWB TD nature of GPR units allowed for these systems to locate reflecting layers and objects in a profile, with a high directivity monostatic horn antenna. Once specific reflecting elements had been identified, FFT analyses of these reflections allowed for the study of interactions between incident and reflected radar signals and the scatterers analysed. As the relationship between the sum of the FFTs of individual reflections in a profile and the FFT of the entire profile were identical, this method allowed for a piecewise analysis of FD radar signals, particularly for applications requiring the modelling or near-surface radar truth acquisition of scattering parameters.

FD analyses of TD GPR waveforms and their reflections showed that higher frequencies comprised the reflections that are closest to the antenna, such as vegetation canopy layers, with lower frequencies becoming more dominant with distance and subsequent underlying reflective layers, as expected. Plant canopy layers became more transparent as measurement frequency decreased. The frequency contents of the soil surface where slightly below that of the antenna centre frequency of 1 GHz; subsurface frequency contents were usually lower, with SR being directly and inversely related to surface and subsurface FD σ^0 returns, respectively.

While vegetation canopy in the greenhouse wheat study clearly scattered away L-band frequencies form the soil surface, lower frequency P-band signals were actually confined and directed by vertically oriented canopy elements such as stalks, which resulted in increased returns from the subsurface Al termination beneath, by decreasing air-spreading losses. FFTs of entire profiles from the greenhouse showed clear effects of interactions between returned signals from canopy, surface, and subsurface layers, with evidence of both constructive and destructive interference having occurred.

Field studies showed the effects of strong subsurface termination upon L- and P-band σ^0 values, and showed that under specific conditions FD analysis could further the depth sensitivity of existing radar systems by comparing two or more profile frequency responses.

In conclusion, deconvolution of TD GPR signals to FD allowed for the study of scattering by various components and estimation of σ^0 at the commonly used P- and L-bands in a single sensor, showing the usefulness of broadband TD GPR for calibration of narrowband FD radar applications.

Acknowledgements Funding for the GPR unit was provided in part by Phil Rasmussen, the United States-Israel Binational Agricultural Research and Development Fund (BARD) through project no. IS-2839-97, United States Department of Agriculture, NRI under agreement 2001-01248, and the Utah Agricultural Experimental Station (UAES). The Rocky Mountain Space Grant Consortium, the Dept of Plants, Soils, and Biometeorology, and the School of Graduate Studies at Utah State University are acknowledged for providing a graduate research fellowship. Bill Mace is acknowledged for his assistance with construction and field work. Dr Cynthia M. Furse of the Dept of Electrical and Computer Engineering at the University of Utah is acknowledged for answering signal processing-related questions. Ariel Serbin, Louis Koberstein, Seth Humphries, and others are gratefully acknowledged for their assistance in field work and/or data processing.

REFERENCES

Balanis, C. A. (1982) *Antenna Theory: Analysis and Design*. John Wiley & Sons, Inc., New York, USA.

Berlin, G. L., Tarabzouni, M. A., Al-Naser, A. H., Sheikho, K. M. & Larson, R. W. (1986) SIR-B subsurface imaging of a sand-buried landscape: Al Labbah Plateau, Saudi Arabia. *IEEE Trans. Geosci. Remote Sens*. **GE-24**(4), 595–601.

Blumberg, D. G., Freilikher, V., Kaganovskii, Y. & Maradudin, A. A. (2002) Subsurface microwave remote sensing of soil-water content: field studies in the Negev Desert and optical modelling. *Int. J. Remote Sens.* **23**(19), 4039–4054.

Blumberg, D. G., Freilikher, V., Lyalko, I. V., Vulfson, L. D., Kotlyar, A. L., Shevchenko, V. N. & Ryabokonenko, A. D. (2000) Soil moisture (water content) assessment by an airborne scatterometer: the Chernobyl disaster area and the Negev Desert. *Remote Sens. Environ*. **71**, 309–319.

Daniels, J., Blumberg, D. G., Vulfson, L. D., Kotlyar, A. L., Freilikher, V., Ronen, G. & Ben-Asher, J. (2003) Microwave remote sensing of physically buried objects in the Negev desert: Implications for subsurface Martian exploration. *J. Geophys. Res. Planets* **108**(E4), 8033.

Dobson, M. C. & Ulaby, F. T. (1986a) Active microwave soil moisture research. *IEEE Trans. Geosci. Remote Sens*. **GE-24**(1), 23–36.

Dobson, M. C. & Ulaby, F. T. (1986b) Preliminary evaluation of the SIR-B response to soil moisture, surface roughness and crop canopy cover. *IEEE Trans. Geosci. Remote Sens*. **GE-24**(4), 517–526.

Du, Y., Ulaby, F. T. & Dobson, M. C. (2000) Sensitivity to soil moisture by active and passive microwave sensors. *IEEE Trans. Geosci. Remote Sens*. **38**(1), 105–114.

Dubois, P. C., van Zyl, J. & Engman, T. (1995) Measuring soil moisture with imaging radars. *IEEE Trans. Geosci. Remote Sens*. **33**(4), 915–926.

Fung, A. K. (1994) *Microwave Scattering and Emission Models and Their Applications*. Artech House, Boston, Massachusetts, USA.

Lambot, S., Rhebergen, J., van den Bosch, I., Slob, E. C. & Vanclooster, M. (2004a) Measuring the soil water content profile of a sandy soil with an off-ground monostatic ground penetrating radar. *Vadose Zone J*. **3**, 1063–1071.

Lambot, S., Slob, E. C., van den Bosch, I., Stockbroeckx, B. & Vanclooster, M. (2004b) Modeling of ground penetrating radar for accurate characterization of subsurface dielectric properties. *IEEE Trans. Geosci. Remote Sens.* **42**, 2555–2568.

Oh, Y., Sarabandi, K. & Ulaby, F. T. (1994) An inversion algorithm for retrieving soil moisture and surface roughness from polarimetric radar observations. In: *IGARSS '94 Surface and Atmospheric Remote Sensing: Technologies, Data Analysis and Interpretation*, 1582–1584. IEEE, Pasadena, California, USA.

Paloscia, S. (2002) A summary of experimental results to assess the contribution of SAR for mapping vegetation biomass and soil moisture. *Can. J. Remote Sens.* **28**(2), 246–261.

Serbin, G. & Or, D. (2003) Near-surface soil water content measurements using horn antenna radar—methodology and overview. *Vadose Zone J.* **2**, 500–510.

Serbin, G. & Or, D. (2004) GPR measurement of crop canopies and soil water dynamics- implications for radar remote sensing. In: *Tenth Int. Conf. on Ground Penetrating Radar* (GPR 2004) (ed. by E. C. Slob, A. Yarovoy & J. Rhebergen), 497–500. Delft University of Technology, Delft, The Netherlands.

Serbin, G. & Or, D. (2005) Radar measurement of wheat canopy and underlying surface water content dynamics. *Remote Sens. Environ*. **96**(1), 119–134.

Topp, G. C., Davis, J. L. & Annan, A. P. (1980) Electromagnetic determination of soil water content: Measurements in coaxial transmission lines. *Water Resour. Res.* **16**(3), 574–582.

Ulaby, F. T. (1999) *Fundamentals of Applied Electromagnetics*. Prentice Hall, Upper Saddle River, New Jersey, USA.

Ulaby, F. T., Dubois, P. C. & van Zyl, J. (1996) Radar mapping of surface soil moisture. *J. Hydrol.* **184**, 57–84.